Electronic Supplementary Material (ESI) for Physical Chemistry Chemical Physics.

Supporting information for: Designing and Understanding Microporosity in Liquids

Gavin Melaugh,[†] Nicola Giri,[‡] Christine E. Davidson,[‡] Stuart L. James,[‡] and Mario G. Del Pópolo[*,†,¶]

Atomistic Simulation Centre, School of Mathematics and Physics, Queen's University Belfast, BT7 1NN, UK, School of Chemistry and Chemical Engineering, Queen's University Belfast, BT9 5AG, UK, and CONICET & Instituto de Ciencias Básicas, Universidad Nacional de Cuyo, Mendoza, Argentina

E-mail: m.del-popolo@qub.ac.uk

[*]To whom correspondence should be addressed
[†]Atomistic Simulation Centre, School of Mathematics and Physics, Queen's University Belfast, BT7 1NN, UK
[‡]School of Chemistry and Chemical Engineering, Queen's University Belfast, BT9 5AG, UK
[¶]CONICET & Instituto de Ciencias Básicas, Universidad Nacional de Cuyo, Mendoza, Argentina

Contents

1 Force-field model and simulation details

Empirical force-fields are extensively used to simulate a wide variety of organic and biological molecules and, despite occasional failures, they provide a fairly reliable description of these materials. Popular force-fields approximate the potential energy of the system, $\mathscr{U}$, with the following analytical formula:

$$\begin{aligned}\mathscr{U} = &\sum_b \frac{k_{r,b}}{2}(r_b - r_{0,b})^2 + \sum_a \frac{k_{\theta,a}}{2}(\theta_a - \theta_{0,a})^2 + \sum_d \sum_{m=1}^{n} \frac{V_{m,d}}{2}[1 + (-1)^{m+1}\cos(m\varphi_d)] \\ &+ \sum_i \sum_j \left\{ 4\varepsilon_{ij}\left[\left(\frac{\sigma_{ij}}{r_{ij}}\right)^{12} - \left(\frac{\sigma_{ij}}{r_{ij}}\right)^{6}\right] + \frac{1}{4\pi\varepsilon_0}\frac{q_i q_j}{r_{ij}} \right\} \end{aligned} \quad (1)$$

The first three terms in this expression are stretching, bending, and dihedral potentials, that define the topology and shape of the molecule, as well as its vibrational and conformational states. The last two terms account for Coulombic and dispersion interactions which, according to standard rules, are computed between atoms located in different molecules and atom pairs belonging to same molecule provided they are separated by four or more covalent bonds. In addition, non-bonded interactions between atoms separated exactly by four chemical bonds are scaled by 0.5. Cross Lennerd-Jones parameters are computed according to the following mixing rules: $\sigma_{ij} = \sqrt{\sigma_i \sigma_j}$ and $\varepsilon_{ij} = \sqrt{\varepsilon_i \varepsilon_j}$.

In our simulations an all-atom model was used to represent the cage cores, while hydrocarbon chains were modelled as united-atom beads. Except for some partial charges the force-field parameters were taken from OPLS-AA and OPLS-UA.[1,2] The force field parameters are listed in Section 9.

Initial configurations for the simulated annealing trajectories were prepared by positioning the molecules in a cubic lattice inside a expanded simulation box, condensing the system at high temperature and pressure, and running a 6 ns NPT simulation at 700 K and 1 bar. Each system was subsequently annealed from 600 K to 200 K at a constant rate of 4 K/ns. Configurations were sampled at various target temperatures and used as starting points for 100 ns-long NPT runs. Table 1 lists system sizes and temperatures explored.

Table 1: N_m: number of molecules; N_a: number of atoms per molecule; T: temperatures.

	N_m	N_a	T
n-C_5	64	132	350 375 400 425 450 500
n-C_{12}	64	216	350 375 400 425 450 500
n-C_{20}	64	312	350 375 400 425 450 500
iso-C_{13}	64	228	350 375 400 425 450 500
neo-C_7	64	156	350 375 400 425 450 500
neo-C_{14}	64	240	350 375 400 425 450 500
neo-C_{22}	64	336	350 375 400 425 450 500

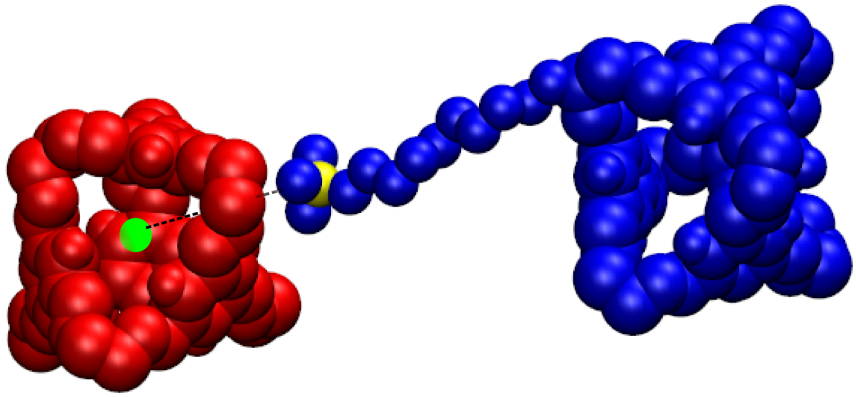

Figure 1: Reaction coordinate snapshot from an umbrella sampling window during the calculation of the cage-tail potential of mean force. Only the cage cores of the two tagged molecules are shown. Molecule 1 is shown in red and molecule 2 is shown in blue. The cage centre of molecule 1, $\mathbf{r}_1^c$, is shown as the green sphere. The tagged tail of molecule 2 is also shown with the tail terminal group, $\mathbf{t}_2$, shown in yellow. The reaction coordinate, $q = |\mathbf{r}_1^c - \mathbf{t}_2|$, is represented by the dashed black line.

2 Free energy calculations

In order to investigate the energetics of the cage occupation process we computed the potentials of mean force (PMF) for a tail terminal group to go inside a neighbouring cage at 400 K. The free energy profiles were calculated using the umbrella sampling/WHAM method under NVT conditions. The reaction coordinate, q, for this process was defined to be the distance between the cage centre of one molecule, molecule 1, and the tail terminal group of a neighbouring molecule, molecule 2. This reaction coordinate is given by

$$q = |\mathbf{r}_1^c - \mathbf{t}_2|, \tag{2}$$

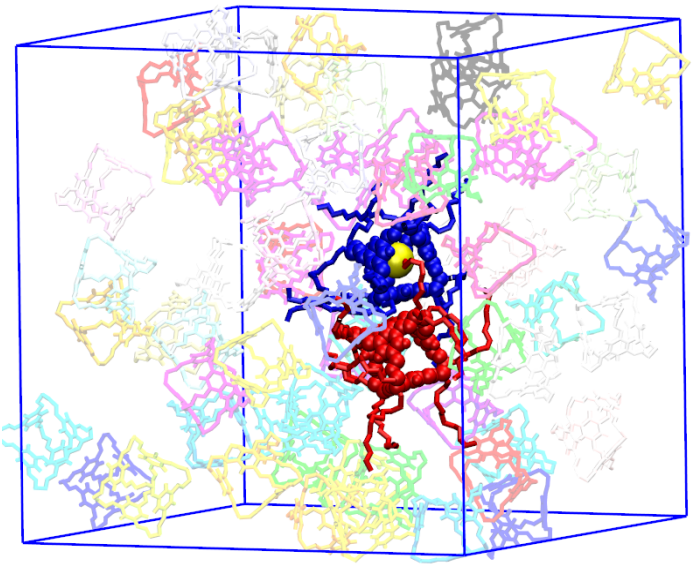

Figure 2: Configurational snapshot of *n*-C12 during a 400 K umbrella sampling window trajectory in which $q = 0$. Molecules 1 and 2 are highlighted in red and blue. The cages of molecules 1 and 2 are represented as spheres to emphasise their structure. The tagged tail terminal group, $\mathbf{t}_2$, of molecule 2 is highlighted with a yellow sphere. At $q = 0$, the tail terminal group is inside the cage. All tails not belonging to molecules 1 and 2 are removed for clarity.

where $\mathbf{r}_1^c$ marks the centre of geometry of the cage, and $\mathbf{t}_2$ is the branching point of the tail terminal group in one of the twelve tails of molecule 2. Figure 1 shows a configuration of the two tagged molecules at a particular value q' of the reaction coordinate q. An actual bulk configuration, from the first umbrella sampling window, where $q = 0$ (*i.e.* the tail $\mathbf{t}_2$ is inside the cage of molecule 1), is shown in Figure 2.

After the WHAM analysis,[3,4] the resulting free-energy function was corrected according to

$$PMF(q)_{true} = PMF(q)_{WHAM} + 2k_BT \ln q, \tag{3}$$

where the term $2k_BT \ln q$ accounts for the increasing volume of configurational space for increasing q.[5]

Prior to performing the umbrella sampling simulations, suitable starting configurations had to be generated for each of the windows. These configurations were generated in an iterative manner so as to minimise any perturbation to an already well equilibrated system. The procedure is as follows:

- Take the final configuration from the 500 K *NPT* simulation.

- Identify two neighbouring cage molecules, close together, that are not occupied.
- Define the centre of geometry of the cage core of the first of these molecules $\mathbf{r}_1^c$.
- Identify a tail, $\mathbf{t}_2$, in molecule 2 that is approximately 1.76 nm from $\mathbf{r}_1^c$.
- If no tail is approximately 1.76 nm from $\mathbf{r}_1^c$, then identify a tail that provides a q value as close to 1.76 nm as possible. Perform constrained molecular dynamics[6] using a value of 1.76 nm to attain the appropriate distance.
- Having attained a q value of 1.76 nm, perform constrained MD for 100 ps using a time-step of 0.001 ps and desired q value of 1.76 nm.
- Use the final configuration from the 1.76 nm simulation for an identical constrained MD simulation with desired q value of 1.74 nm.
- Use the final configuration from the 1.74 nm simulation as input for another constrained MD simulation with desired q value of 1.72 nm.
- Repeat this process until there is a configuration at every 0.02 nm between 0 nm and 1.76 nm.

Note that for the umbrella sampling simulations, only some of the configurations generated from the above procedure were used as starting configurations.

Equipped with the information provided by the cage-tail radial distribution functions, and using a process of trial and error, we decided to use 56 umbrella sampling windows for the computation of the PMF in the range $0 \leq q \leq 1.80$. These 56 windows partitioned the reaction coordinate into three regions, each with the same window spacing and force constant. The window parameters for the three different regions are summarised in Table 2.

Table 2: Umbrella windows information for computing the potential of mean force.

Range	N° of Windows	Window Interval [nm]	κ [kJ mol^{-1} nm^{-2}]
0.00-0.78 nm	40	0.02	10000
0.80-1.12 nm	8	0.04	5000
1.20-1.76 nm	8	0.08	1000

Having attained suitable starting configurations, and decided on the appropriate partitioning of the reaction coordinate, 10 ns equilibration simulations were carried out in each window. These simulations involved a 5 ns annealing from 600-400 K at a rate of 5 K/350 ps, and a 5 ns continuation at 400 K. After equilibration, 15 ns umbrella sampling simulations were carried out at 400 K.

3 Effective interaction between two isolated cages

The effective interaction between two isolated alkyl-substituted iminospherand cages was assessed by computing the potential of mean force (PMF) to bring two molecules together. Only the neo-series was investigated. These PMF were calculated by taking the centre of mass of one cage core, $\mathbf{r}_{c,1}$, towards the centre of mass of another cage core, $\mathbf{r}_{c,2}$. The PMF were computed using the umbrella sampling/WHAM methods described in the previous section. The reaction coordinate to compute the effective intermolecular potential was given by $q = |\mathbf{r}_{c,2} - \mathbf{r}_{c,1}|$

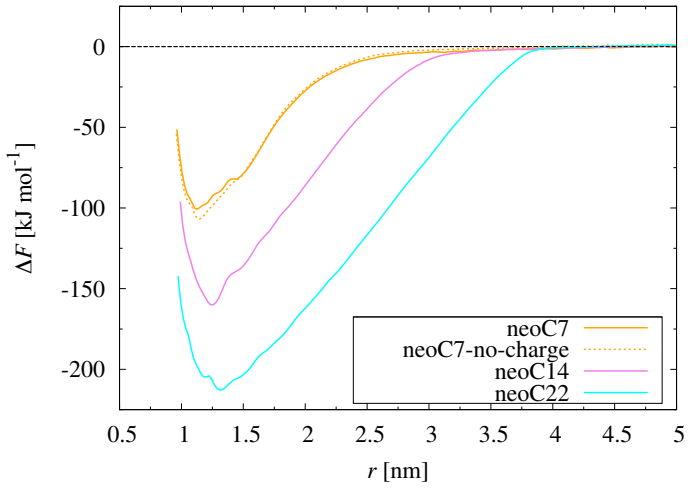

Figure 3: Potentials mean force between two molecules of the neo-systems separated by a distance q. Calculations performed at 400 K. The dashed orange line shows the PMF for neo-C_7 when the atomic charges are all set to zero.

The umbrella sampling simulations were performed at 400 K, using a time-step of 0.001 ps, with no periodic boundary conditions and no cut-offs. Prior to performing umbrella sampling simulations, suitable starting configurations were generated for each window. A force constant, κ, of 1000 kJ mol^{-1}nm^{-2} was used in all cases. Having generated the appropriate starting configurations, 50 ns umbrella sampling simulations were performed at each window. The first

10 ns were used as equilibration, while the remaining 40 ns provide the data for the WHAM analysis.

The resulting intermolecular PMF are shown in Figure 3. The most obvious feature in this figure is the increasing depth of the free energy minimum with increasing tail length. This is merely a manifestation of the increased number of atoms that accompanies the increase in the size of the molecules. However, the curvature of the PMF well decreases with increasing tail length, pointing to a softer interaction potential as the tails get longer.

The alkyl substituted iminospherand cages are hybrids between aromatic and aliphatic hydrocarbons. One may expect that cohesion is then mostly determined by dispersion forces, molecular volume and chain flexibility, with electrostatic interactions playing a secondary role. In order to test this hypothesis the free-energy required to bring two isolated neo-C_7 molecules together was computed using the full atomistic model discussed above, and setting all the atomic charges to zero. The results shown in Figure 3 demonstrate that electrostatic interactions contribute very little to the binding free energy.

4 Thermodynamical properties

Figure 4 shows the average configurational energy as a function of temperature,$U(T)$, obtained during simulated annealing simulations at P=1bar, for the cage systems considered in figure 3 of the paper. The black dots represent linear fits, $f(T) = a + bT$, to the $U(T)$ functions, calculated by least squares in the 250-300 K interval. Table 3 collects the values of a and b.

Table 3: Fitting parameters calculated by least squares from the $U(T)$ curves of Figure 4

System	b [kJ mol^{-1} K^{-1} molecule^{-1}]	a [kJ mol^{-1} molecule^{-1}]
n-C_5	1.8585	-253.25
n-C_{12}	3.4464	-910.74
n-C_{20}	5.3123	-1632.4
neo-C_7	2.1224	-148.16
neo-C_{14}	3.5922	-741.09
neo-C_{22}	5.4822	-1520.3

Figure 5 shows the average volume per molecule as a function of temperature for all the

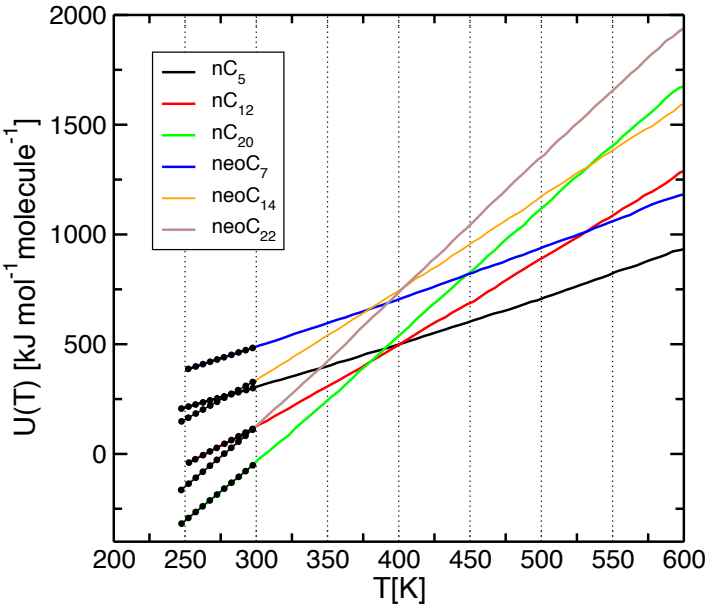

Figure 4: Average configurational energy as a function of temperature,$U(T)$, for the systems considered in figure 3 of the paper.

systems considered in figure 3 of the paper. The change of slope in the $V(T)$ curves has been highlighted by subtracting a linear function, fitted in the 250-300 K interval, from all the curves. The transition temperatures are identified by the intersection of the dotted lines, and the resulting values are very close to those revealed by the $U(T)$. Note that these results can be sensitive to the cooling rate of the simulated annealing procedure (4K/ns), and therefore the transition temperatures may change slightly when using different cooling rates.

5 Tail-tail radial distribution functions

Figure 6(a) to (c) show the tail-tail radial distribution functions (RDF), $g_{tt}(r)$, for the short, medium, and long tailed systems at 500 K, 450 K, and 400 K. These distributions point to a disordered, liquid-like arrangement amongst the tail terminal groups. The effect of temperature on the structural ordering of the tails is slight, which suggests that either the tails exhibit similar levels of fluidity at all the temperatures considered, or that the tails exhibit similar levels of frozen disorder. Looking at each plot individually, we see that the structural ordering of the tail terminal groups in the $n-$systems is different from that of the bulkier $neo-$systems. One of the most striking features of Figure 6(a) to (c) is that the tail-tail RDF for the three tail lengths are

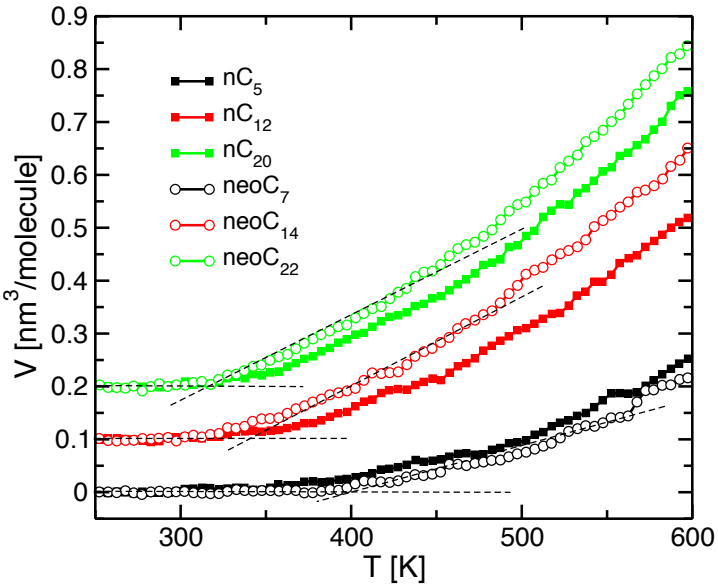

Figure 5: Molar volume as a function of temperature $V(T)$ for the cage systems considered in Figure 3 of the paper.

almost identical. There is essentially no difference in the $g_{tt}(r)$ as the tail length increases.

6 Tail length statistics

To gain further insight into the structure of the hydrocarbon tails, we calculated radial distribution functions, $g_{tp}(r)$, between the pivot atom of the terminal group and its corresponding attachment point at the vertex of the cage. These functions provide some insight into the flexed and extended states of the tails. Figure 7 and its inset show the $g_{tp}(r)$ for the neo systems at both 400 K and 500 K. The first thing to note is that the longer tailed systems allow for sampling of larger tail pivot distances. The inset of Figure 7 highlights the broadening of the distributions with increasing tail length. The bimodal nature of the tail-pivot distributions suggests that there are two prefered conformational states of the tails. In neo-C_7, the two very well-defined peaks at 0.48 nm and 0.53 nm suggest that the tails are, on average, in an extended conformation. In neo-C_{14} the maximum tail length extension is approximately 1.4 nm. The maximum in the tail-pivot RDF, at 1.16 nm, suggests that a significant proportion of the tails are in a conformation that is almost fully extended. The larger width of the distribution in neo-C_{14}, however, suggests that there are less tails, on average, in an extended conformation in comparison with neo-C_7. The first smaller peak in the tail-pivot RDF of neo-C_{14}, at 0.6 nm, points to a population of

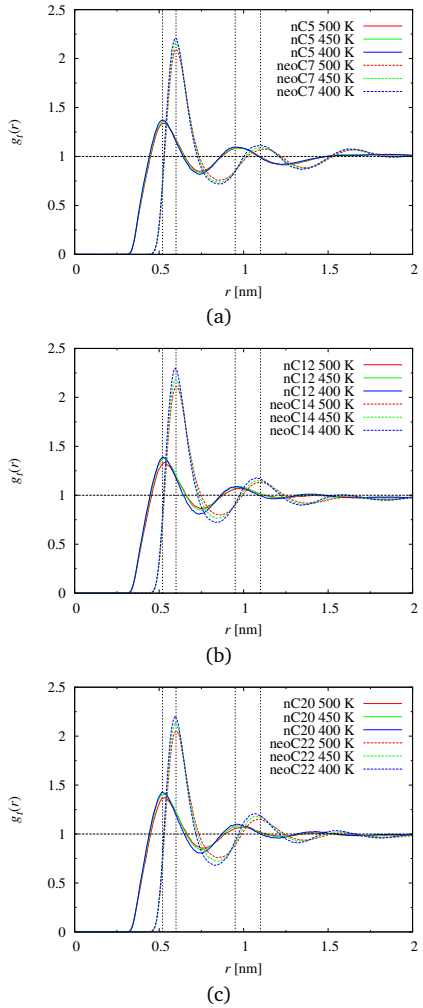

Figure 6: Tail-tail radial distribution functions for the short, medium, and long tailed systems at 500 K, 450 K, and 400 K: (a) nC5 and neoC7. (b) nC12 and neoC14. (c) nC20 and neoC22. Dashed vertical lines show the location of the main peaks.

tails in a half extended conformation. In neo-C_{22}, the distribution is more diffuse due to a more diverse sampling of the tail-pivot distances. The maximum tail length extension in neo-C_{22} is approximately 2.4 nm. The peak in the tail-pivot RDF, located at 1.8 nm, suggests that many tails are in a conformation that is 75% of the maximum tail length extension. The other peak, at 0.6 nm, suggests that there is also a population of tails that are in a conformation that is 25% of the maximum tail length extension. Looking particularly at the distributions of neo-C_{14} and neo-C_{22}, there is a tendency for the distributions to become less structured as the temperature increases.

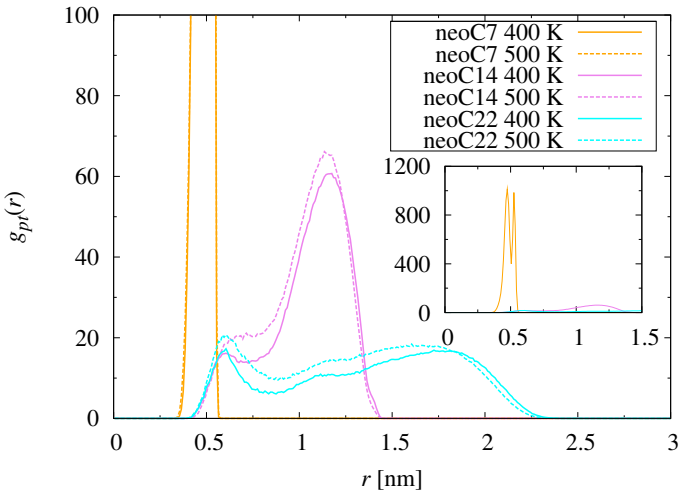

Figure 7: Tail-pivot radial distribution functions,$g_{tp}(r)$, for the neo terminated systems at 500 K and 400 K. The inset has a larger y scale to emphasise the broadening of the distributions with increasing tail length.

7 MD Studies of Methane/n-C_5 Mixtures

The initial mixed system consisted of 64 n-C_5 molecules plus 100 methane molecules inserted randomly into the fluid (x_{CH_4} =0.61). A local relaxation procedure was then applied to the initial configuration, followed by a simulated annealing run with a starting temperature of 600 K. Sample configurations were taken from the annealing trajectory at 400 K and 350 K. The 400 K configuration was used as the starting point for a 100 ns NPT run at the same temperature. 50 methane molecules were then randomly removed from the system to yield a methane concentration of x_{CH_4} =0.44, and a further 25 methane molecules were removed to yield the mixed system with x_{CH_4} =0.28. MD simulations of the 50- and 25-methane-molecule systems were also run at 400 K. The 25-methane-molecule system was also run at 350 K. All simulations were run with the same control parameters used for the pure liquids. Methane was modelled with the force-field reported in Table 8, Table 9 and Table 10.

Figure 8 (a) to (c) show the cage occupation data for the mixed systems of n-C_5 at 400 K. Also plotted is the time evolution of the number of tails that occupy cage cavities. The occupation data in the n-C_5 system with 100 methane molecules (Figure 8(a)) shows that there are, on average, 61 occupied cages. On average, there are 40 occupying tails in this system, and 25 occupying CH_4 molecules. A careful analysis of the MD trajectory reveals that methane molecules generally occupy cages in which no tails are present. That is to say, the methane

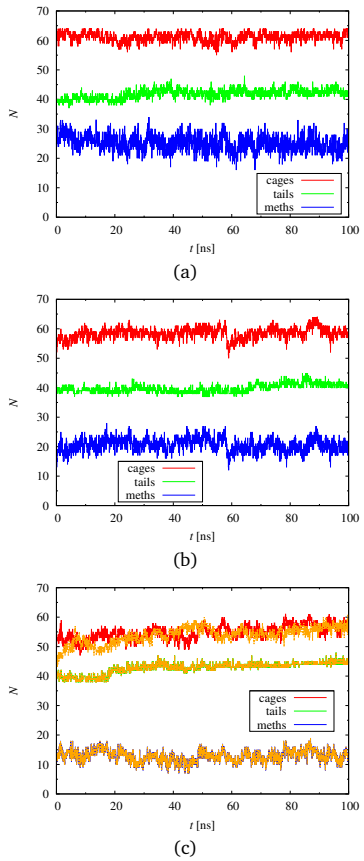

Figure 8: Occupation data for n-C_5 mixed with varying concentrations of methane at 400 K showing the number of occupied cages (cages), the number of occupying tails (tails), and the number of occupying methane molecules (meths). All systems contain 64 n-C_5 cage molecules each with 12 tails of 5 carbon atoms long: (a) 100 methane molecules. (b) 50 methane molecules. (c) 25 methane molecules. In (c), the orange curves denote the corresponding occupation data at 350 K and suggest very little temperature effect. Note that the quantities reported are system size specific.

molecules occupy the free cage cores apart from the cavities available in the intermolecular space. In the system with 50 methane molecules (Figure 8(b)) we see that the average number of occupied cages is now 58, and that the average number of occupying tails is again approximately 40. Therefore the decrease in the number of occupied cages is due to the decrease in the number of occupying CH_4 molecules, which we see is now approximately 20. The decreasing concentration leads to a decreasing number of occupying methane molecules, and hence a subsequent reduction in the number of occupied cages. This trend is completed when we consider the system with 25 methane molecules (Figure 8(c)). The average number of occupying CH_4 molecules is approximately 15, and the number of occupied cages falls to approximately 53. There is also a very slight drift in the number of occupying tails. Clearly, cage occupation by

CH_4 is more dynamic than cage occupation by tails. High concentrations of methane cause all available cage cores to be occupied. Figure 8(c) also shows the corresponding occupation data of the 25 methane molecule system at 350 K (orange lines). Evidently the reduction in temperature from 400 K to 350 K does not affect the occupation of cages by tails or methane molecules.

8 Grand Canonical Simulations

There is a degree of ambiguity associated with the equilibrium concentration of methane in the MD gas mixture simulations in the previous section. To overcome this ambiguity, we performed Grand Canonical Monte Carlo (GCMC) simulations on three systems that exhibited different cage occupation behaviour, n-C_5, n-C_{12}, and neo-C_{14}. We chose a temperature of 350 K, as we wanted to maximise the contribution to gas absorption from the cage cores. In these stochastic simulations, methane molecules were randomly inserted or removed from the system according to the acceptance criteria for the Grand Canonical ensemble.[6] Given that at low temperature (350 K) the large cage molecules display a very slow dynamics, canonical moves (intramolecular moves, and molecular translations and rotations) lead to a very large rejection rate. Consequently only grand canonical moves were considered in the simulations, i.e. insertion and deletion of gas molecules. Static configurations were obtained from NPT molecular dynamics simulations of the pure systems (no gas molecules) at 350 K. For each system, 20 GCMC simulations were performed at pressures 0.1, 0.2, 0.3, 0.4, ..., and 2.0 atm. For each pressure the same static configuration was used. To circumvent the lack of canonical sampling, the 20 simulations were repeated using 10 different static configurations. Each of the static configurations were obtained from different points of the corresponding MD trajectory. Therefore, for each configuration 10 different isotherms were calculated and subsequently averaged to give the average isotherms of Figure 11. For each pressure point, an initial equilibration run was carried out. These runs were 3×10^6 MC steps long, which proved to be sufficient to equilibrate the concentation of gas molecules in the system. After equilibration, 6×10^6 MC steps production runs were carried out

References

[1] Jorgensen, W. L.; Maxwell, D. S.; Tirado-Rives, J. *J. Am. Chem. Soc.* **1996**, *118*, 11225–11236.

[2] Jorgensen, W. L.; Tirado-Rives, J. *Proc. Nat. Ac. Sci. USA* **2005**, *102*, 6665–6670.

[3] Roux, B. *Comput. Phys. Commun.* **1995**, *91*, 275–282.

[4] Kumar, S.; Rosenberg, J. M.; Bouzida, D.; Swendsen, R. H.; Kollman, P. A. *J. Comput. Chem.* **1992**, *13*, 1011 – 1021.

[5] H.Zheng,; Zhang, Y. *J. Chem. Phys* **2008**, *128*, 204106.

[6] Frenkel, D.; Smit, B. *Understanding Molecular Simulation*, 2nd ed.; Academic Press, Inc., 2001.

9 Appendix

Table 4: Atom type parameters for the alkylated cages.

Atom type	Mass	Charge [e]	σ [nm]	ε [kJ mol^{-1}]
CB	12.011	0.000	0.3550	0.2929
CA	12.011	-0.115	0.3550	0.2929
HC	1.008	0.115	0.2420	0.1255
CU	13.019	0.265	0.3500	0.3347
NU	14.007	-0.597	0.3250	0.7113
CH	13.019	0.332	0.3850	0.3347
C2	14.027	0.000	0.3905	0.4937
C3	15.035	0.000	0.3905	0.7322
CI	13.019	0.000	0.3850	0.3347
CF	15.035	0.000	0.3910	0.6694
CT	12.011	0.000	0.3800	0.2092
CP	15.035	0.000	0.3960	0.6067

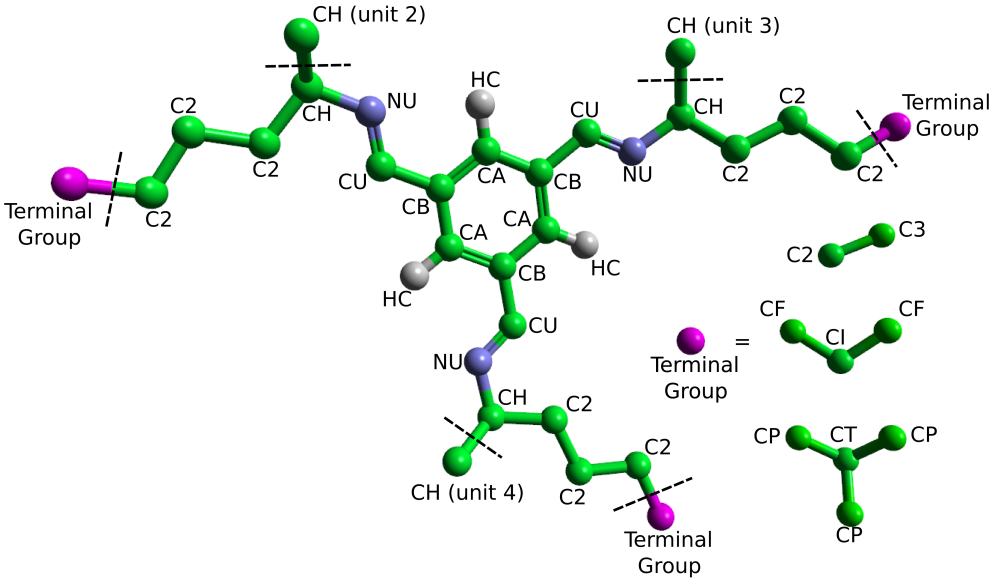

Figure 9: Repeating unit for the model of any alkylated cage molecule. Green spheres denote all atom or united atom carbons, blue spheres denote nitrogen, and grey spheres denote benzene hydrogens. Dashed lines at CH groups denote a connection to another identical unit. Dashed lines at C2 groups denote connections to terminal groups. System with longer tails have more C2 groups before the terminal group. The pink spheres represent the different types of terminal group. These are shown at the bottom right of the picture. The force-field parameters are listed in Table 4,Table 5,Table 6, and Table 7.

Table 5: Bond stretching parameters for the alkylated cages.

Bond Type	k_r [kJ mol^{-1} nm^{-2}]	r_{eq} [nm]
CB-CA	392459.2	0.1400
CA-HC	284512.0	0.1080
CB-CU	357313.6	0.1481
CU-NU	282001.6	0.1250
NU-CH	282001.6	0.1451
CH-CH	217568.0	0.1526
CH-C2	217568.0	0.1526
C2-C2	217568.0	0.1526
C2-C3	217568.0	0.1526
C2-CI	217568.0	0.1526
CI-CF	217568.0	0.1526
C2-CT	259408.0	0.1526
CT-CP	259408.0	0.1526

Table 6: Angle bending parameters for the alkylated cages.

Angle Type	k_θ [kJ mol^{-1} rad^{-2}]	θ_{eq} [°]
CB-CA-CB	711.28	120.0
CB-CA-HC	292.88	120.0
CA-CB-CA	711.28	120.0
NU-CU-CB	585.76	120.0
CU-CB-CA	585.76	120.0
CH-CH-NU	669.44	109.0
CH-NU-CU	585.76	119.4
C2-CH-NU	669.44	109.0
C2-CH-CH	527.18	111.5
CH-C2-C2	527.18	112.4
C2-C2-C2	527.18	112.4
C3-C2-C2	527.18	112.4
CI-C2-C2	527.18	112.4
CF-CI-C2	527.18	112.4
CF-CI-CF	527.18	111.5
CT-C2-C2	527.18	112.4
CP-CT-C2	334.72	109.5
CP-CT-CP	334.72	109.5

Table 7: Dihedral potential parameters for the alkylated cages

Dihedral Type	C_1 [kJ mol^{-1}]	C_2 [kJ mol^{-1}]	C_3 [kJ mol^{-1}]	C_4 [kJ mol^{-1}]
CA-CB-CA-HC	0.000	30.334	0.000	0.000
CB-CA-CB-CA	0.000	30.334	0.000	0.000
CU-CB-CA-CB	0.000	30.334	0.000	0.000
CU-CB-CA-HC	0.000	30.334	0.000	0.000
NU-CU-CB-CA	0.000	30.334	0.000	0.000
NU-CH-CH-NU	46.170	-4.050	1.130	0.000
CH-CH-NU-CU	-4.184	-1.464	0.000	0.000
CH-NU-CU-CB	0.000	836.800	0.000	0.000
C2-CH-NU-CU	-4.184	-1.464	0.000	0.000
C2-CH-CH-NU	-11.807	5.786	12.565	0.000
C2-CH-CH-C2	-14.226	5.230	12.970	0.000
C2-C2-CH-NU	-11.807	5.786	12.565	0.000
C2-C2-CH-CH	-14.226	5.230	12.970	0.000
CH-C2-C2-C2	-14.226	5.230	12.970	0.000
C2-C2-C2-C2	-14.226	5.230	12.970	0.000
C3-C2-C2-C2	-14.226	5.230	12.970	0.000
CI-C2-C2-C2	-14.226	5.230	12.970	0.000
CF-CI-C2-C2	-14.226	5.230	12.970	0.000
CT-C2-C2-C2	-14.226	5.230	12.970	0.000
CP-CT-C2-C2	-14.226	5.230	12.970	0.000

Table 8: Atom type parameters for methane.

Atom type	Mass	Charge [e]	σ [nm]	ε [kJ mol^{-1}]
CT	12.011	-0.240	0.3550	0.2761
HH	1.008	0.060	0.2500	0.1255

Table 9: Bond stretching parameters for methane

Bond Type	k_r [kJ mol^{-1} nm^{-2}]	r_{eq} [nm]
CT-HH	284512.0	0.1090

Table 10: Angle bending parameter for methane

Angle Type	k_θ [kJ mol^{-1} rad^{-2}]	θ_{eq} [°]
HH-CT-HH	276.1440	107.80

Synthetic supporting information for: Designing and Understanding Microporosity in Liquids

Gavin Melaugh,[†] Nicola Giri,[‡] Christine E. Davidson,[‡] Stuart L. James,[‡] and Mario G. Del Pópolo,[†]

Atomistic Simulation Centre, School of Mathematics and Physics, Queen's University Belfast, BT7 1NN, UK, School of Chemistry and Chemical Engineering, Queen's University Belfast, BT9 5AG, UK, and CONICET & Instituto de Ciencias Básicas, Universidad Nacional de Cuyo, Mendoza, Argentina

E-mail: m.del-popolo@qub.ac.uk

Contents

1. General experimental details for synthesis and characterisation

Reactions that required anhydrous or inert conditions were performed under an inert atmosphere of dry nitrogen using Schlenk line techniques. All other reactions were fitted with a dying tube filled with blue silica gel. Solutions or liquids were prepared in round bottom flasks or pear shaped flasks and transferred using oven dried syringes through rubber septa. Reactions were stirred magnetically using Teflon-coated stir bars. Heating of reactions was carried out using an electrically heated silicon oil bath or a heat block from which the temperature specified is the temperature of the bath or block. Solvents were removed using a rotary evaporator at water aspirator pressure or under high vacuum.

Dry tetrahydrofuran was distilled under nitrogen from sodium benzophenone ketyl radical when required and similarly dry dichloromethane was distilled over calcium hydride. Other solvents were used without distillation form chemical suppliers. Solvents for extractions and chromatography were of technical grade. Flash chromatography was performed using Merck Silica (230-400 mesh) and all analysis was carried out using Merck Silica gel 60 plates. Results were visualised by UV-light (λ = 254 nm) and/ or staining with potassium permanganate solution, cerium ammonium molybdate (CAM), 2,4-dinitrophenylhydrazine, followed by heating.

1,3,5-Triformylbenzene was prepared by previously described standard literature procedures. (*R,R*)-1,2-bis(2-hydroxyphenyl)-1,2-diaminoethane was purchased from Diamoniopharm. All other chemicals were purchased from Sigma-Aldrich and used as received.

^{1}H, ^{13}C, H-COSY and HMQC NMR spectra were obtained using a Bruker AM 300MHz or 500MHz and referenced to the appropriate solvent. Chemical shifts (δ) are displayed in parts per million (ppm) and coupling constants are calculated in Hz. The Analytical Service in the School of Chemistry (ASEP) carried out elemental analysis of compounds using a Perkin-Elmer 2400 CHN microanalyser. Mass spectrometry was carried out by ASEP using Micromass MALDI-TOF mass spectrometer using CHCA as a matrix and electrospray mass spectrometry using Waters LCT Premier™ XE benchtop orthogonal acceleration time-of-flight (oa-TOF) mass spectrometer. The EPSRC National Mass Spectrometry Service Centre (NMSSC) in Swansea carried out MALDI-TOF of two samples using DHB and dithranol as a matrix.

Compounds were characterised by thermogravimetric analysis (TGA) on a Q5000IR analyser (TA instruments) with an automated vertical overhead thermobalance at a heating rate of 5 ^{o}C per min. Differential Scanning Calorimetry (DSC) was used to determine melting points on a Q2000 DSC at a heating/cooling rate of 10^{o}C per min. The visual melting pictures were taken on a hot-stage Olympus BX 50 Phase Pol Darkfield Microscope.

2. **Synthetic details for n-C_{12}**

***(S,S)-N,N'*-bis(salicylidene)-1,2-dodecanyl-1,2-diaminoethane**

Tridecanal (1.70 g, 8.5 mmol) was added to a solution of *(R,R)*-1,2-bis(2-hydroxyphenyl)-1,2-diaminoethane (1.0 g, 4.1 mmol) in toluene (12.5 ml) at ambient temperature. The resulting solution was refluxed overnight with a Dean-Stark trap. After removal of the solvent under reduced pressure, the resulting viscous yellow oil was purified by column chromatography (eluent cyclohexane: dichloromethane 3:2). 1.46 g of yellow oil was obtained (yield 59%).

^{1}H-NMR (300 MHz, $CDCl_3$): δ 13.49 (br s, 2H, ArOH), 8.25 (s, 2H, Imine H), 7.28 (ddd, $^3J_{HH}$ = 9Hz, $^4J_{HH}$ =1.5 Hz 2H, ArH), 7.20 (dd, $^3J_{HH}$ =9 Hz, 2H, ArH), 6.96 (d, $^3J_{HH}$= 9 Hz, 2H, ArH), 6.84 (ddd, $^3J_{HH}$ = 9 Hz, 2H, ArH), 3.27 (m, 2H, C*H), 1.66 (m, 4H), 1.22 (m, 40H), 0.87 (t, $^3J_{HH}$ = 9 Hz, 6H).

^{13}C-NMR (75 MHz, $CDCl_3$): δ 165.2, 161.7, 132.6, 131.7, 118.9, 118.9, 117.5, 74.1, 32.9, 32.3, 30.0, 30.0, 29.9, 29.8, 29.7, 26.6, 23.1, 14.5.
MS (ES^+) 605 ($[M+H]^+$).

***(S,S)*-1,2-dodecanyl-1,2-diaminoethane**

To a clear, yellow solution of *(S,S)-N,N'*-bis(salicylidene)-1,2-dodecanyl-1,2-diaminoethane (8.48 g, 14.0 mmol) in 60 ml of THF was added a mixture of 4.2 ml of 37% HCl solution and 60 ml of THF. After stirring at r.t. for 24 hrs, the mixture was cooled down in ice to give white precipitate which was filtered and basified with 1M NaOH. The aqueous layer was allowed to reflux for 1hr after which the organic layer was extracted three times with 30 ml of DCM and dried over dry Na_2SO_4 to yield 0.13 g of diamine (yield 68%) as a white solid.

^{1}H-NMR (300 MHz, $CDCl_3$): δ 2.53 (bs, 2H, NC*H), 1.44-1.26 (m, 48H), 0.88 (t, $^3J_{HH}$ = 12 Hz, 6H).

^{13}C-NMR (75 MHz, $CDCl_3$): δ55.6, 35.5, 32.3, 30.2, 30.0, 29.7, 27.0, 23.1, 14.5.
MS (ES^+) 397 ($[M+H]^+$).

***n*-Dodecanyl cage, n-C_{12}**

(S,S)-1,2dodecanyl-1,2-diaminoethane (0.160g, 0.40 mmol) was dissolved in 2.5 ml of $CHCl_3$ and TFB (0.037 g, 0.22 mmol) dissolved in 2.5 ml $CHCl_3$ and trifluoroacetic acid (0.006 ml, 0.075 mmol) were added. After heating the reaction mixture at 60^{o}C for 1.5 weeks, the solvent was removed under reduced pressure. The crude was dissolved in the minimum amount of acetone and allowed to precipitate using ice. The solid was then purified by column chromatography (9:1, cyclohexane: ethyl acetate) to give a yellow waxy solid 0. 05 g (26.7 % yield).

^{1}H-NMR (300 MHz, $CDCl_3$): δ 8.05 (s, 12H), 7.87 (s, 12H), 3.32 (d, $^{3}J_{HH}$ = 9Hz, 12H), 1.77 (m, 24 H), 1.22 (m, 240H), 0.87 (t, $^{3}J_{HH}$ = 6 Hz, 36 H).

^{13}C-NMR (125 MHz, $CDCl_3$): δ 159.7, 136.9, 129.9, 75.8, 32.3, 30.0, 29.9, 29.7, 26.8, 23.0, 14.5.
MS (MALDI-TOF^{+}) 2813 ([M+H]$^{+}$)
CHN analysis for $C_{192}H_{336}N_{12}$: C 81.98, H 12.04, N 5.98 ; found C 80.83, H 11.77, N 5.83

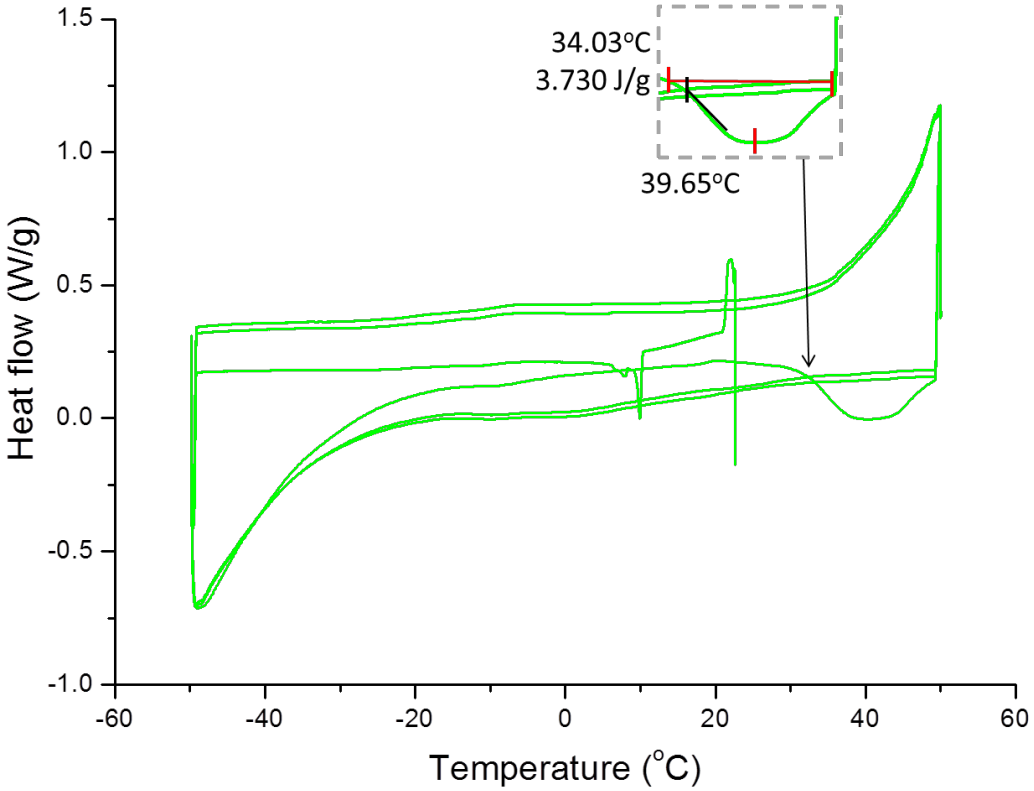

Figure S1 DSC of **n-C_{12}** (exotherms shown as positive heat flow).

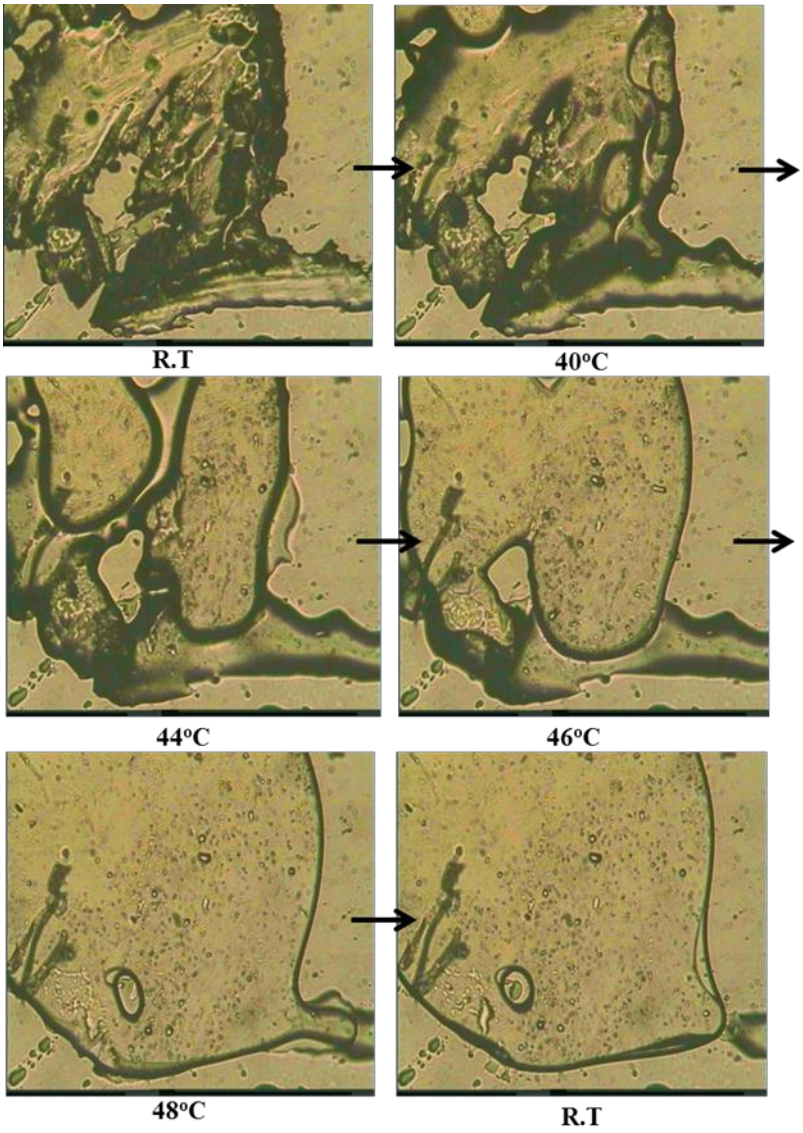

Figure S2 Visual melting of **n-C_{12}** on a hot stage microscope.

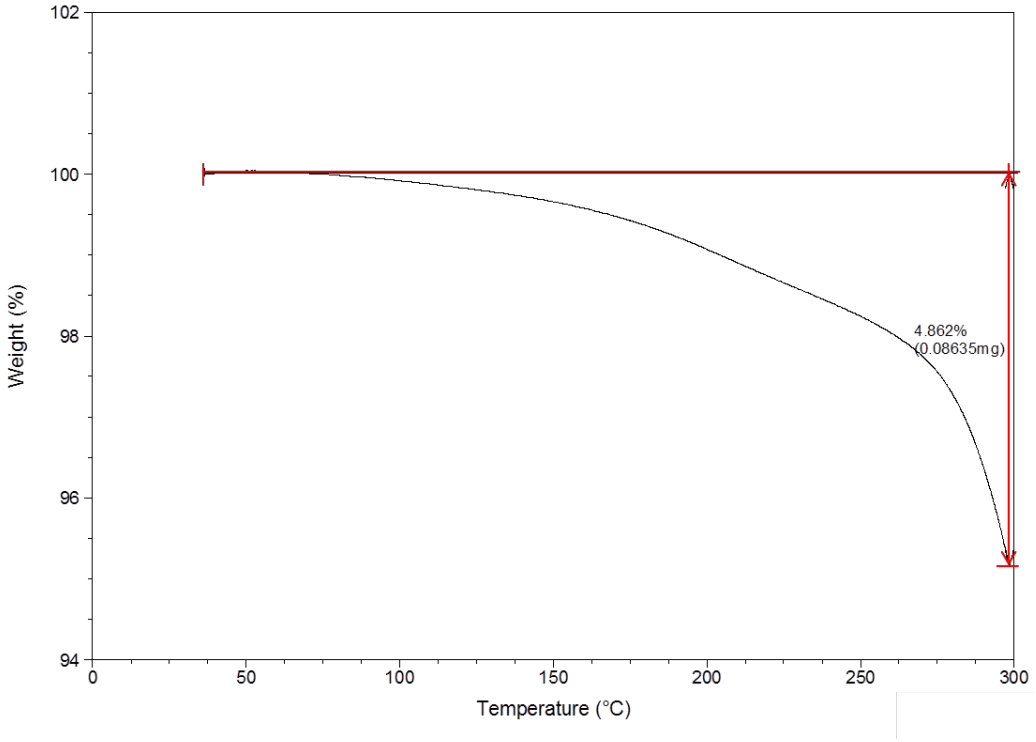

Figure S3 Thermogravimetric analysis of **n-C_{12}**

3. **Synthetic details for i-C_{13}**

Dilithium tetrachlorocuprate

$$CuCl_2 + 2LiCl \xrightarrow{THF} Li_2CuCl_4$$

Lithium chloride (0.38 g, 9.0 mmol) previously dried at 145°C in high vacuum was suspended in 6 ml of dry THF in a Schlenk tube with stirring. To the suspension copper(II) chloride (0.59 g, 4.4 mmol) was added under nitrogen to obtain an intense red-brown solution.

12-Methyl-1-tridecanol

3-Bromopropane (2.5 ml, 26.3 mmol) was slowly added dropwise to a suspension of Mg turnings (0.8 g, 31.0 mmol) in dry THF (12 ml) vigorously stirred, to maintain a steady reflux. Once the exothermic reaction has subsided, the mixture was stirred for 30 min. to have an homogeneous grey suspension. The *iso*propyl magnesium bromide solution was cooled at -78°C and then the solution of 11-bromoundecanol (1.0 g, 4.0 mmol) in THF (4 ml) was added, followed by the solution of dilithium tetrachlorocuprate. The mixture was allowed to warm to r.t. and stirred for 2 hrs, resulting in a purple-black suspension. The reaction was quenched with saturated aqueous ammonium chloride solution and extracted with ethyl acetate. The organic phase was washed with saturated aqueous sodium bicarbonate solution and brine, and dried over anhydrous magnesium sulfate. The crude alcohol was purified by flash column-cromatography using petroleum ether/ethyl acetate = 9/1 as eluent. (colourless liquid, 0.920 g, yield 96%).

^{1}H-NMR (300 MHz, $CDCl_3$): δ 3.64 (t, 2H, $^3J_{HH}$ = 6 Hz), 1.63-1.05 (m, 22H), 0.86 (d, 6H, $^3J_{HH}$ = 6 Hz).

^{13}C-NMR (75 MHz, $CDCl_3$): δ 63.1, 39.2, 32.9, 30.1, 29.8, 29.8, 29.7, 29.6, 28.1, 27.5, 25.9, 22.8.

12-Methyl-1-tridecanal

DMSO (0.63 ml, 8.92 mmol) was dissolved in dry CH_2Cl_2 (15 ml), cooled to -78°C and treated with oxalyl chloride (0.38 ml, 4.53 mmol). After stirring at this temperature for 30 min., a solution of 12-methyl-1-tridecanol (0.760 g, 3.54 mmol) in CH_2Cl_2 (5 ml) was added dropwise. The stirring was continued for further 30 min., followed by addition of Et_3N (2.5 ml, 17.84 mmol). The reaction was stirred at -78°C for 15 min. and then allowed to heat up to r.t. The mixture was diluted with Et_2O and

washed with ammonium chloride saturated solution, brine and dried over magnesium sulfate. Purification by column chromatography (Pentane/Diethyl Ether = 9/1) gave 0.594 g of pure 12-methyl-1-tridecanal (Yield 79 %).

^{1}H-NMR (300 MHz, $CDCl_3$): δ 9.77 (t, 1H, $^{3}J_{HH}$ = 2 Hz), 2.42 (td, 2H, $^{3}J_{HH}$ = 7 Hz, $^{3}J_{HH}$ = 2 Hz), 1.67-1.11 (m, 19 H), 0.86 (d, 6H, $^{3}J_{HH}$ = 6 Hz).

^{13}C-NMR (75 MHz, $CDCl_3$): δ 203.4, 44.3, 39.4, 30.3, 30.1, 29.9, 29.8, 29.7, 29.6, 28.4, 27.8, 23.0, 22.5.

(*S*,*S*)-*N*,*N*'-bis(salicylidene)-1,2-(11-methyl-dodecanyl)-1,2-diaminoethane

12-Methyl-1-tridecanal (2.170 g, 10.20 mmol) was added to a solution of (*R*,*R*)-1,2-bis(2-hydroxyphenyl)-1,2-diaminoethane (1.084 g, 4.44 mmol) in toluene (25 ml) at ambient temperature. The resulting solution was refluxed overnight with a Dean-Stark trap. After removal of the solvent under reduced pressure, the resulting viscous yellow oil was purified by column chromatography (Cyclohexane/DCM: 7/3→6/4→5/5) (1.100 g, yield 39%)

^{1}H-NMR (300 MHz, $CDCl_3$): δ 13.48 (s, 2H), 8.25 (s, 2H), 7.31-7.25 (m, 2H), 7.20 (dd, $^{3}J_{HH}$ =9 Hz, $^{4}J_{HH}$ =1 Hz, 2H), 6.97 (d, $^{3}J_{HH}$= 6 Hz, 2H), 6.84 (ddd, $^{3}J_{HH}$ = 6 Hz, $^{4}J_{HH}$ =1 Hz, 2H), 3.30-3.24 (m, 2H), 1.66 -1.11 (m, 42 H), 0.85 (d, $^{3}J_{HH}$ = 6 Hz, 12H).

^{13}C-NMR (75 MHz, $CDCl_3$): δ 165.2, 161.7, 132.6, 131.7, 118.9, 118.8, 117.5, 74.1, 39.4, 33.0, 30.3, 30.1, 30.0, 29.9, 29.8, 28.4, 27.8, 26.7, 23.1.

MS (ES^+) 633 ($[M+H]^+$).

(*S*,*S*)- 1,2-(11-methyl-dodecanyl)-1,2-diaminoethane

(*S*,*S*)-*N*,*N*'-bis(salicylidene)-1,2-(11-methyl-dodecanyl)-1,2-diaminoethane (0.476 g, 0.75 mmol) was dissolved in a 1:1 mixture of THF/CH_3CN (10 ml). To the yellow solution HCl 37% was added and the solution stirred overnight. The white precipitate formed, was filtered off, redissolved in THF and precipitated again adding CH_3CN in an ice bath. The white precipitate was then dissolved in NaOH 1M, extracted with chloroform and dried over Na_2SO_4. Filtration and removal of the solvent under reduced pressure gave 0.285 g of pure diamine (Yield 89 %)

^{1}H-NMR (300 MHz, $CDCl_3$): δ 2.53 (bs, 2H,), 1.58-1.11 (m, 46 H), 0.86 (d, $^{3}J_{HH}$ = 6 Hz, 12H).

^{13}C-NMR (75 MHz, $CDCl_3$): δ 55.6, 39.5, 35.4, 30.3, 30.2, 30.1, 30.0, 28.4, 27.8, 27.0, 23.0.

MS (ES^+) 425 ($[M+H]^+$).

Isotridecyl cage, i-C_{13}

(*S*,*S*)-1,2-(11-methyl-dodecanyl)-1,2-diaminoethane (0.285 g, 0.67 mmol) was dissolved in 2.5 ml of $CHCl_3$ and TFB (0.085 g, 0.33 mmol) dissolved in 2.5 ml $CHCl_3$ and trifluoroacetic acid (0.010 ml, 0.13 mmol) were added. After heating the reaction mixture at 65^{o}C for 9 days, the solvent was removed under reduced pressure and the crude purified by column chromatography (Benzene/Ethyl Acetate = 99/1). The residue was then dissolved in a minimum amount of chloroform and acetone was added till the solution became turbid. After standing overnight in the freezer, a white waxy precipitate was formed. After decanting the solvent, the white precipitate was washed with acetone and dried under high vacuum. (0.086 g, yield 35%).

M.p. = 37^{o}C

^{1}H-NMR (500 MHz, $CDCl_3$): δ 8.05 (s, 12H), 7.87 (s, 12H), 3.34-3.29 (m, 12H), 1.8-1.74 (m, 12H), 1.62-1.57 (m, 12H), 1.50 (septuplet, 12H, $^{3}J_{HH}$ = 7 Hz), 1.22-1.06 (m, 216 H), 0.85, (d, $^{3}J_{HH}$ = 7 Hz, 72H).

^{13}C-NMR (125 MHz, $CDCl_3$): δ 159.7, 137.0, 130.0, 75.8, 39.5, 32.2, 30.3, 30.1, 30.0, 29.9, 28.4, 27.8, 26.7, 23.1.

MS (MALDI-TOF) 2981 ([M]$^{+}$).

CHN analysis for $C_{204}H_{360}N_{12}$: C 82.19, H 12.17, N 5.64; found C 82.32, H 10.72, N 5.47.

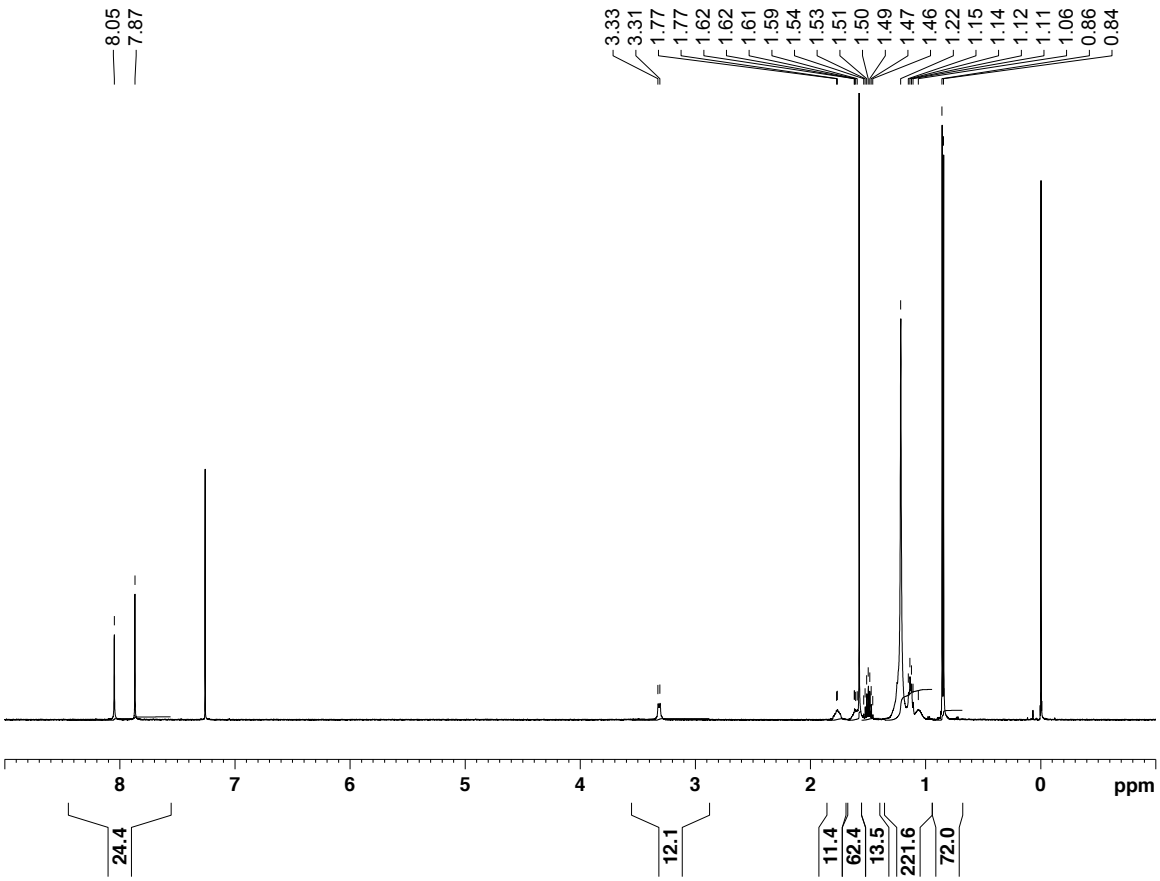

Figure S4. ^{1}H-NMR spectrum (500 MHz, $CDCl_3$) of **i-C_{13}**.

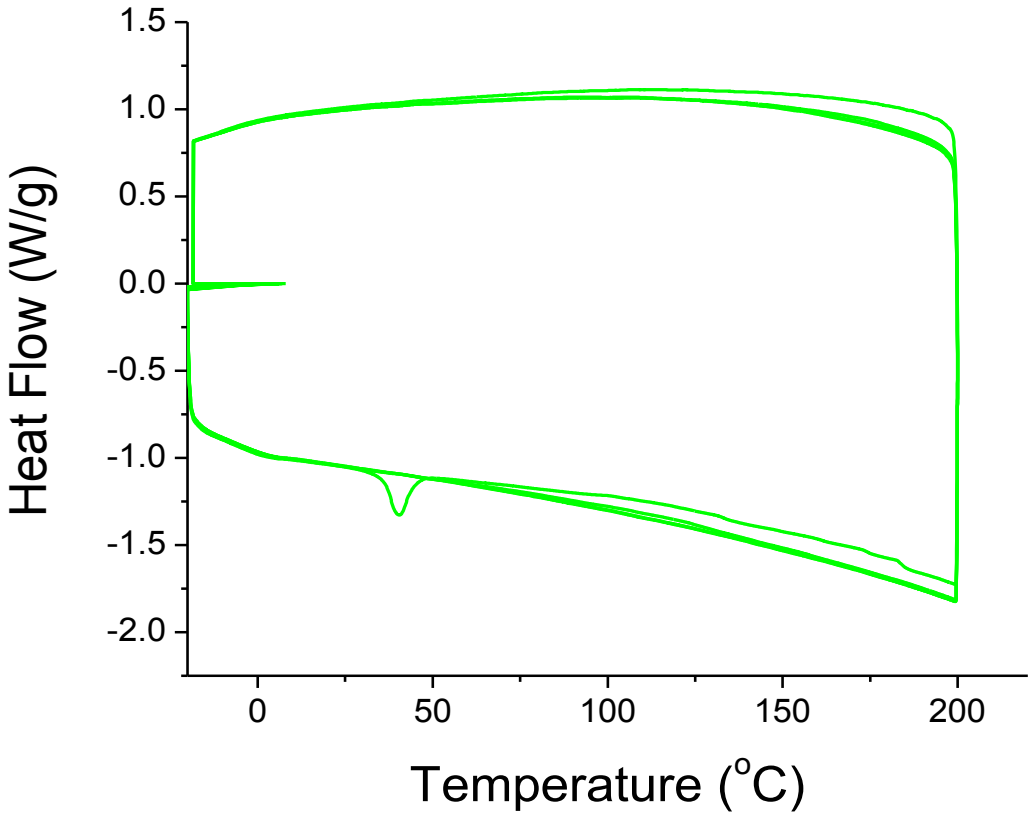

Figure S5. DSC of **i-C_{13}** (exotherms shown as positive heat flow).

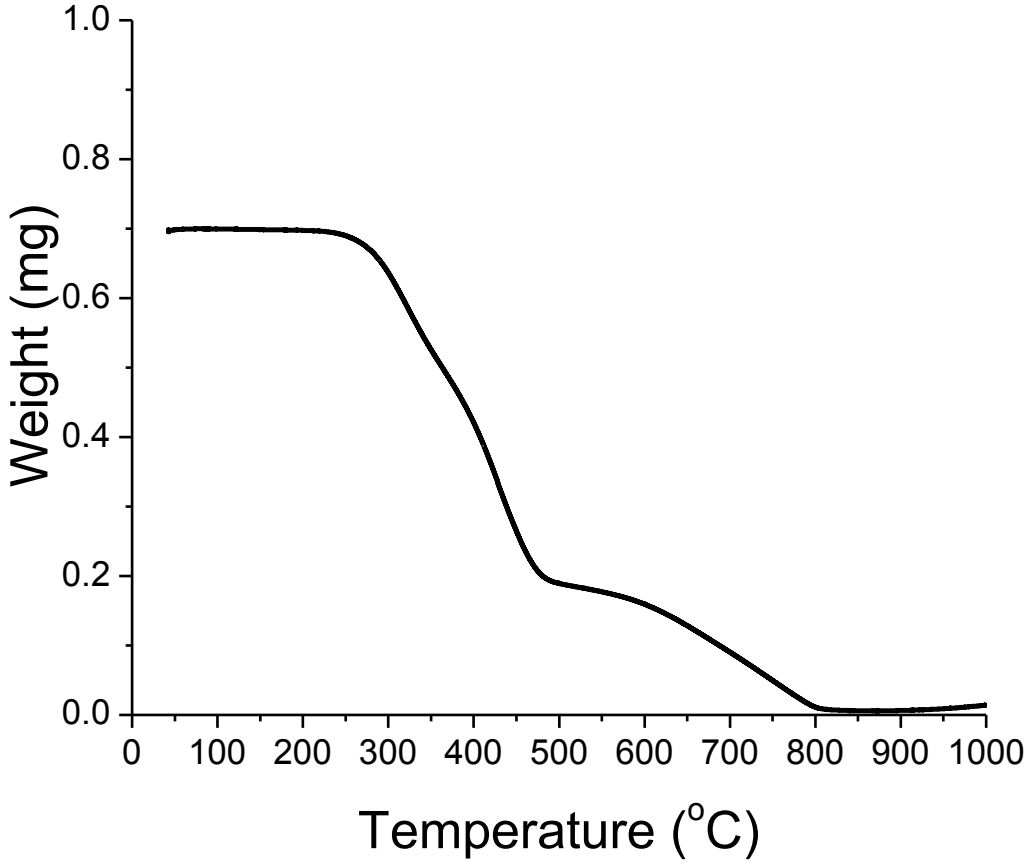

Figure S6. TGA of **i-C_{13}**.

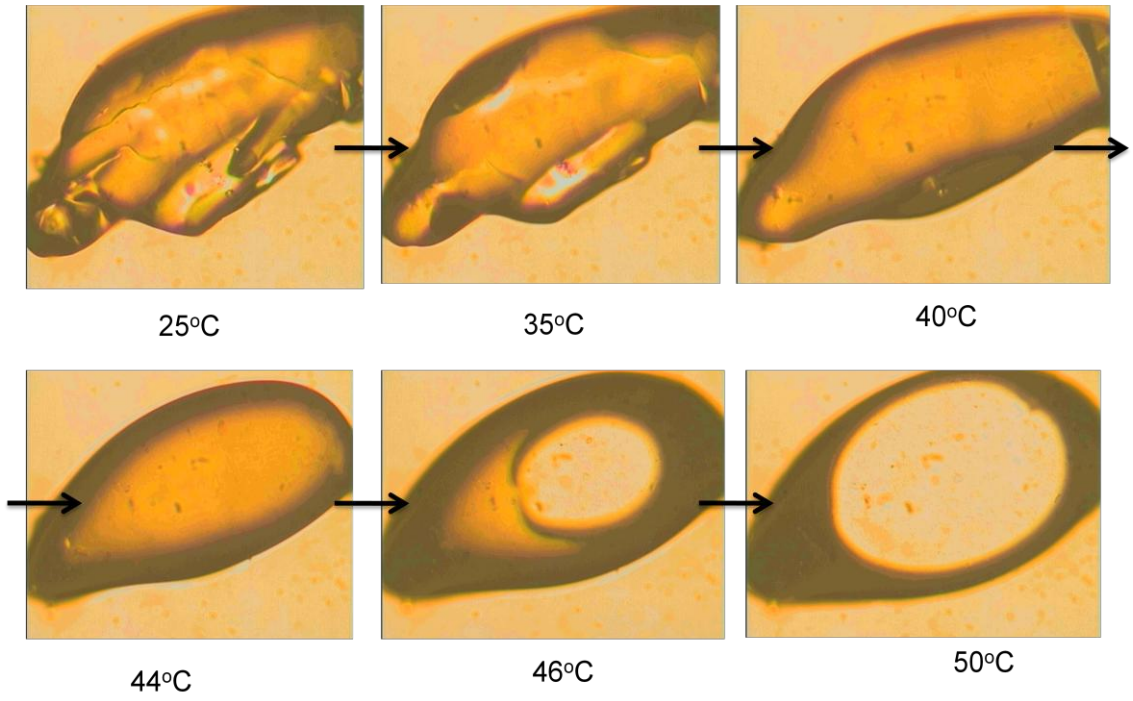

Figure S7. Visual melting of **i-C_{13}** recorded using a hot-stage microscope.

4. Synthetic details for neo-C_{14}

Dilithium tetrachlorocuprate.

Lithium chloride (1..52 g, 36.0 mmol) previously dried at 145°C in high vacuum was suspended in 24 ml of dry THF in a Schlenk tube with stirring. To the suspension copper(II) chloride (2.36 g, 17.5 mmol) was added under nitrogen to obtain an intense red-brown solution.

12-12'-Dimethyl-1-tridecanol

Tert-butylmagnesium chloride 1.0 M in THF (100 ml, 100 mmol) was cooled at -78°C and a solution of 11-bromoundecanol (4.0 g, 15.9 mmol) in anhydrous THF (16 ml) was added, followed by the solution of dilithium tetrachlorocuprate. The mixture was allowed to warm to r.t. and stirred for 2 hrs, resulting in a purple-black suspension. The reaction was quenched with saturated aqueous ammonium chloride solution and extracted with ethyl acetate. The organic phase was washed with saturated aqueous sodium bicarbonate solution and brine, and dried over anhydrous magnesium sulfate. The crude alcohol was purified by flash column-cromatography using petroleum ether/ethyl acetate = 9/1 as eluent. (colourless liquid, 3.63 g, yield 100 %).

^{1}H-NMR (300 MHz, $CDCl_3$): δ 3.64 (t, 2H, $^{3}J_{HH}$ = 6 Hz), 1.63-1.15 (m, 21H), 0.86 (s, 9H).

^{13}C-NMR (75 MHz, $CDCl_3$): δ 63.3, 44.4, 33.0, 30.8, 30.4, 29.9, 29.8, 29.7, 29.6, 25.9, 24.7.

12-12'-Dimethyl-1-tridecanal

DMSO (2.9 ml, 40.17 mmol) was dissolved in dry CH_2Cl_2 (60 ml), cooled to -78°C and treated with oxalyl chloride (1.7ml, 20.4 mmol). After stirring at this temperature for 30 min., a solution of 12-12'-methyl-1-tridecanol (3.64 g, 15.9 mmol) in CH_2Cl_2 (20 ml) was added dropwise. The stirring was continued for further 30 min., followed by addition of Et_3N (11.2 ml, 80.3 mmol). The reaction was stirred at -78°C for 15 min. and then allowed to heat up to r.t. The mixture was diluted with Et_2O and washed with ammonium chloride saturated solution, brine and dried over magnesium sulfate. Purification by column chromatography (Pentane/Diethyl Ether = 9/1) gave 3.6 g of pure 12-12'-dimethyl-1-tridecanal (Yield 100 %).

^{1}H-NMR (300 MHz, $CDCl_3$): δ 9.77 (t, 1H, $^{3}J_{HH}$ = 2 Hz), 2.42 (td, 2H, $^{3}J_{HH}$ = 7 Hz, $^{3}J_{HH}$ = 2 Hz), 1.65-1.15 (m, 18 H), 0.86 (s, 9H).

^{13}C-NMR (75 MHz, $CDCl_3$): δ 203.4, 44.7, 44.3, 31.0, 30.7, 30.1, 30.0, 29.8, 29.7, 29.6, 25.0, 22.5.

(*S*,*S*)-*N*,*N*'-bis(salicylidene)-1,2-(11,11'-dimethyl-dodecanyl)-1,2-diaminoethane

12-12'-Dimethyl-1-tridecanal (6.27 g, 27.7 mmol) was added to a solution of (*R*,*R*)-1,2-bis(2-hydroxyphenyl)-1,2-diaminoethane (2.60 g, 10.6 mmol) in toluene (35 ml) at ambient temperature. The resulting solution was refluxed overnight with a Dean-Stark trap. After removal of the solvent under reduced pressure, the resulting viscous yellow oil was purified by column chromatography (Cyclohexane/DCM: 7/3→6/4→5/5) (2.92 g, yield 42%)

^{1}H-NMR (300 MHz, $CDCl_3$): δ 13.47 (s, 2H), 8.25 (s, 2H), 7.31-7.25 (m, 2H), 7.20 (dd, $^{3}J_{HH}$ =9 Hz, $^{4}J_{HH}$ =1 Hz, 2H), 6.97 (d, $^{3}J_{HH}$= 6 Hz, 2H), 6.84 (ddd, $^{3}J_{HH}$ = 6 Hz, $^{4}J_{HH}$ =1 Hz, 2H), 3.29-3.24 (m, 2H), 1.66 -1.56 (m, 4H), 1.22-1.15 (m, 18H), 0.85 (s, 18H).

^{13}C-NMR (75 MHz, $CDCl_3$): δ 165.2, 161.7, 132.6, 131.7, 118.9, 118.8, 117.5, 74.1, 44.7, 33.0, 31.3, 31.0, 30.7, 30.1, 30.0, 29.9, 29.8, 26.7, 25.0.

MS (ES^{+}) 661 ($[M+H]^{+}$).

(*S*,*S*)- 1,2-(11,11'-dimethyl-dodecanyl)-1,2-diaminoethane

(*S*,*S*)-*N*,*N*'-bis(salicylidene)-1,2-(11,11'-dimethyl-dodecanyl)-1,2-diaminoethane (2.923 g, 4.42 mmol) was dissolved in a 1:1 mixture of THF/CH_3CN (40 ml). To the yellow solution HCl 37% (1.3 ml) was added and the solution stirred overnight. The white precipitate formed, was filtered off, redissolved in THF and precipitated again adding CH_3CN in an ice bath. The white precipitate was then dissolved in NaOH 1M, extracted with chloroform and dried over Na_2SO_4. Filtration and removal of the solvent under reduced pressure gave 0.1.664 g of pure diamine (Yield 83 %)

^{1}H-NMR (300 MHz, $CDCl_3$): δ 2.53 (bs, 2H,), 1.44-1.16 (m, 22 H), 0.86 (s, 18H).

^{13}C-NMR (75 MHz, $CDCl_3$): δ 55.3, 44.3, 35.0, 31.0, 30.6, 30.2, 30.1, 30.0, 30.0, 29.8, 27.0, 25.0.

MS (ES^+) 453 ($[M+H]^+$).

Neotetradecyl cage, neo-C_{14}

(*S*,*S*)-1,2-(11,11'-dimethyl-dodecanyl)-1,2-diaminoethane (1.986 g, 4.38 mmol) was dissolved in 7 ml of $CHCl_3$ and TFB (0.355 g, 2.19 mmol) dissolved in 7 ml $CHCl_3$ and trifluoroacetic acid (0.042 ml, 0.55 mmol) were added. After heating the reaction mixture at 65^{o}C for 18 days, the solvent was removed under reduced pressure and the crude purified by column chromatography (Benzene→Benzene/Ethyl Acetate = 99/1). 1.017 g, of pure cage were obtained (yield 59%).

M.p. = 52^{o}C

^{1}H-NMR (500 MHz, $CDCl_3$): δ 8.05 (s, 12H), 7.87 (s, 12H), 3.34-3.29 (m, 12H), 1.80-1.74 (m, 12H), 1.62-1.57 (m, 12H), 1.22-1.07 (m, 216H), 0.85, (s, 108H).

^{13}C-NMR (125 MHz, $CDCl_3$): δ 159.3, 136.6, 129.6, 75.4, 44.3, 31.8, 30.6, 30.3, 29.7, 29.6, 29.6, 29.5, 29.4, 26.4, 24.6.

MS (MALDI-TOF) 3149 $[M]^+$, 3172 $[M+Na]^+$, 3188 $[M+K]^+$.

CHN analysis for $C_{216}H_{384}N_{12}$: C 82.37, H 12.29, N 5.34; found C 82.42, H 11.92, N 5.38.

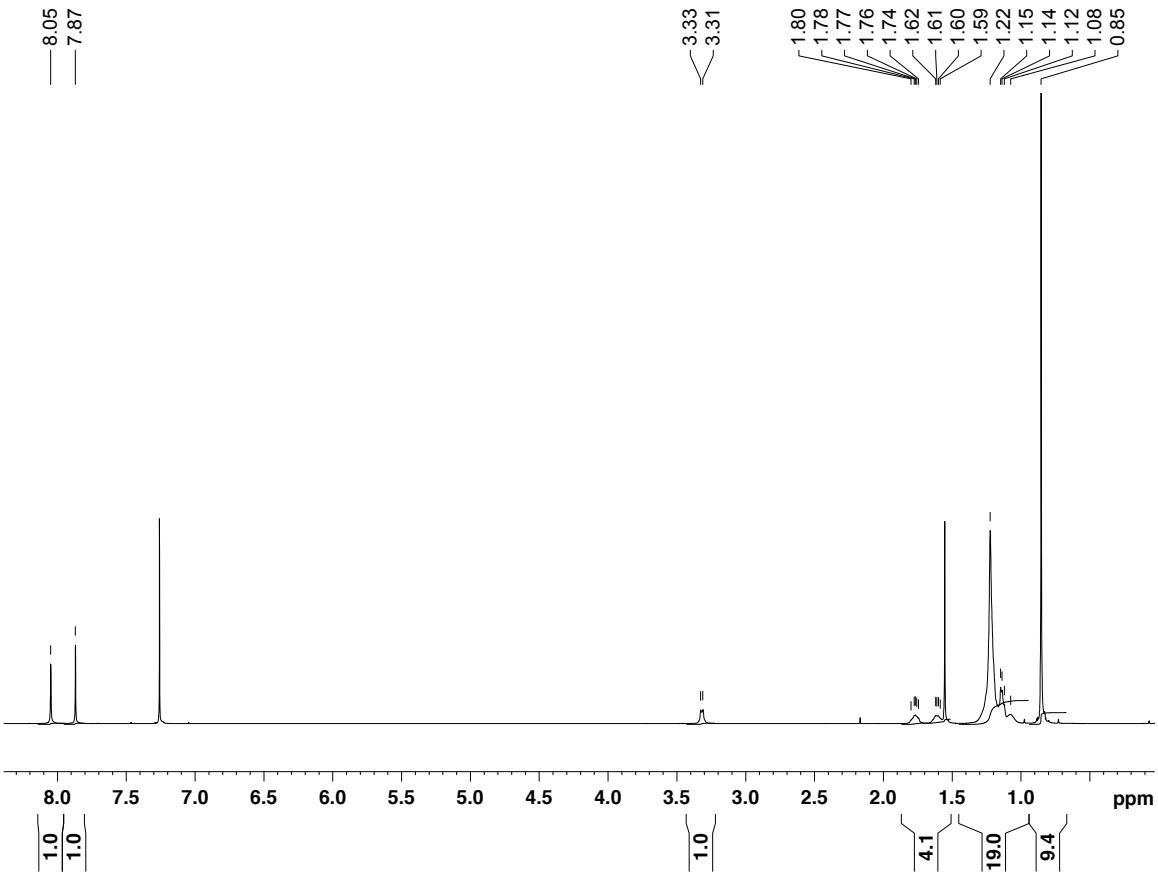

Figure S8. ^{1}H-NMR spectrum (500 MHz, CDCl spectrum) of **neo-C_{14}**.

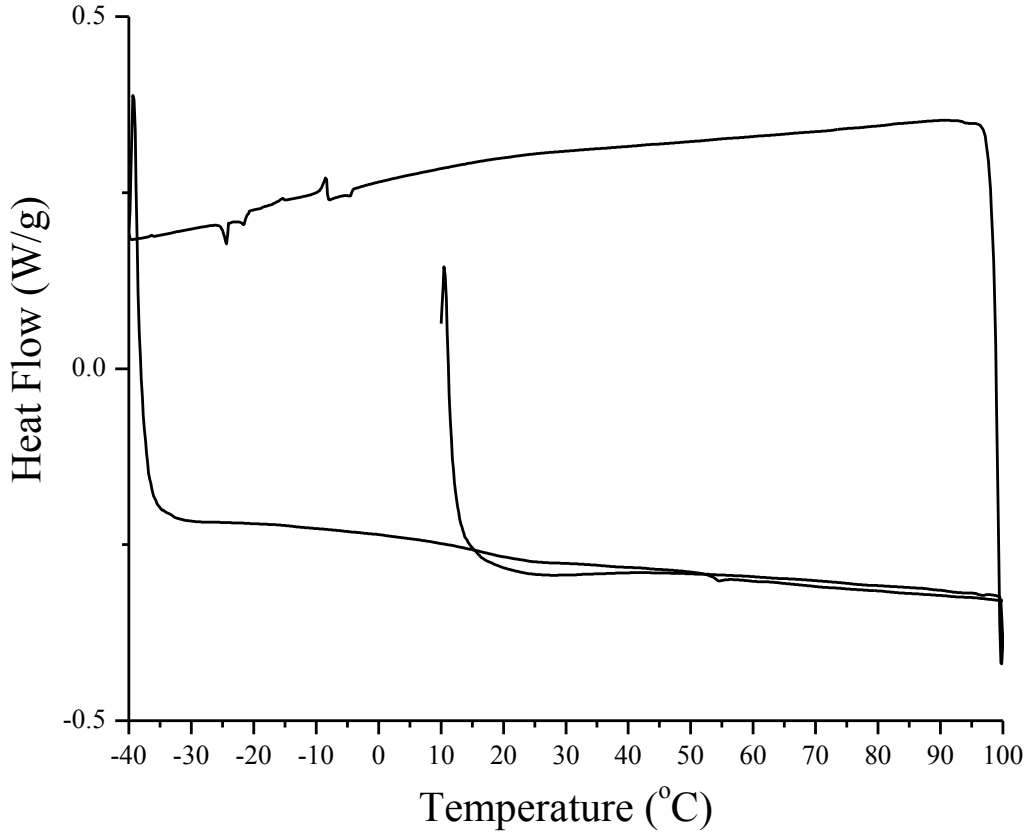

Figure S9. DSC of **neo-C_{14}** (exotherms shown as positive heat flow)

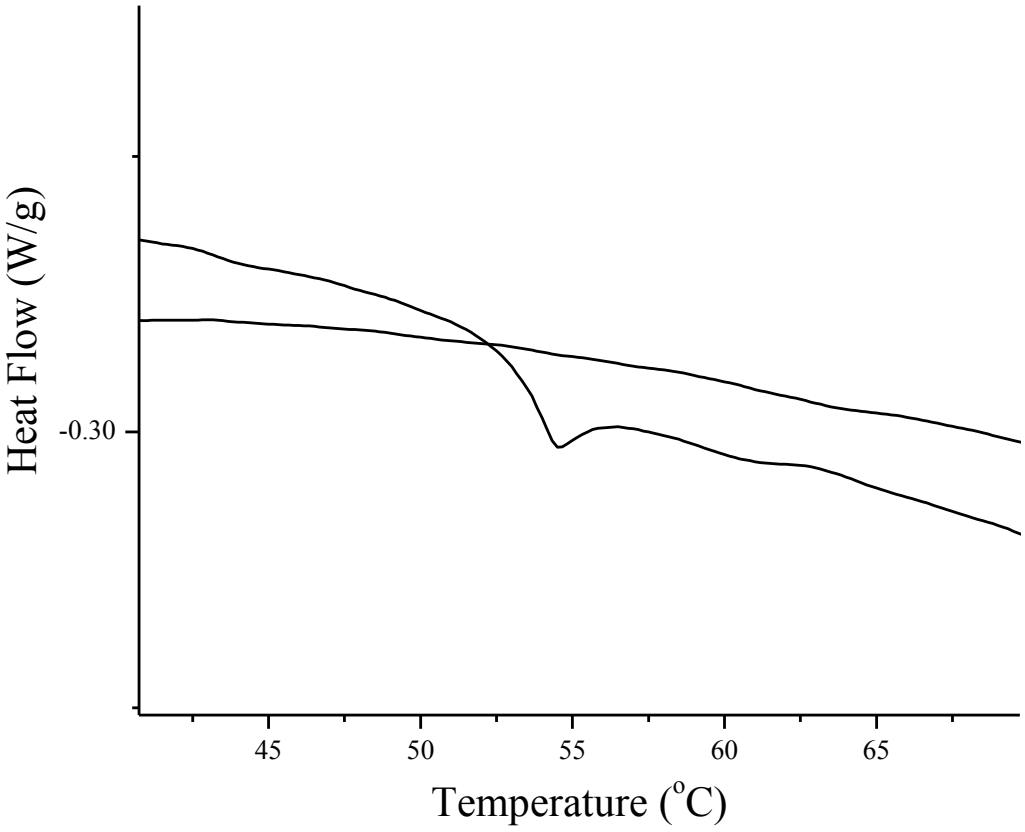

Figure S10. Expansion of DSC of **neo-C_{14}**.

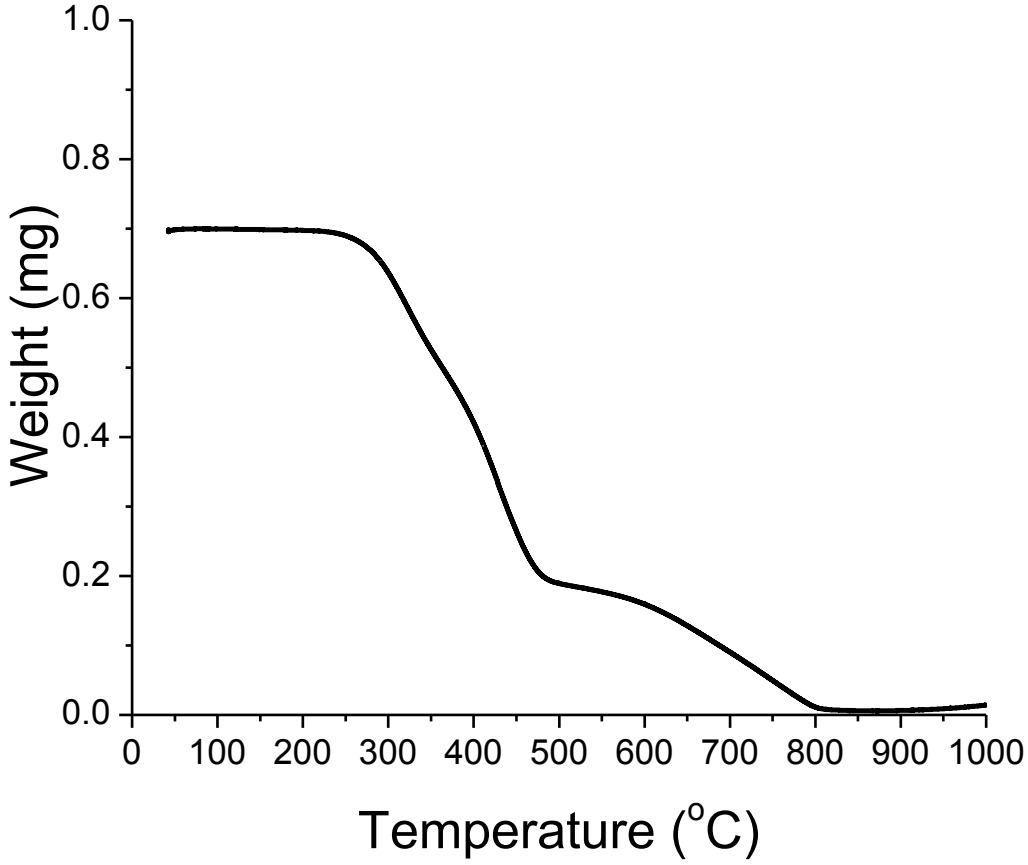

Figure S11. TGA of **neo-C_{14}**.